The defect chemistry and dielectric properties of Sb_2O_3 doped non-stoichiometric barium strontium titanate ceramics

Chen Zhang, Zhixin Ling & Gang Jian

Journal of Materials Science: Materials in Electronics

ISSN 0957-4522

J Mater Sci: Mater Electron
DOI 10.1007/s10854-016-5316-5

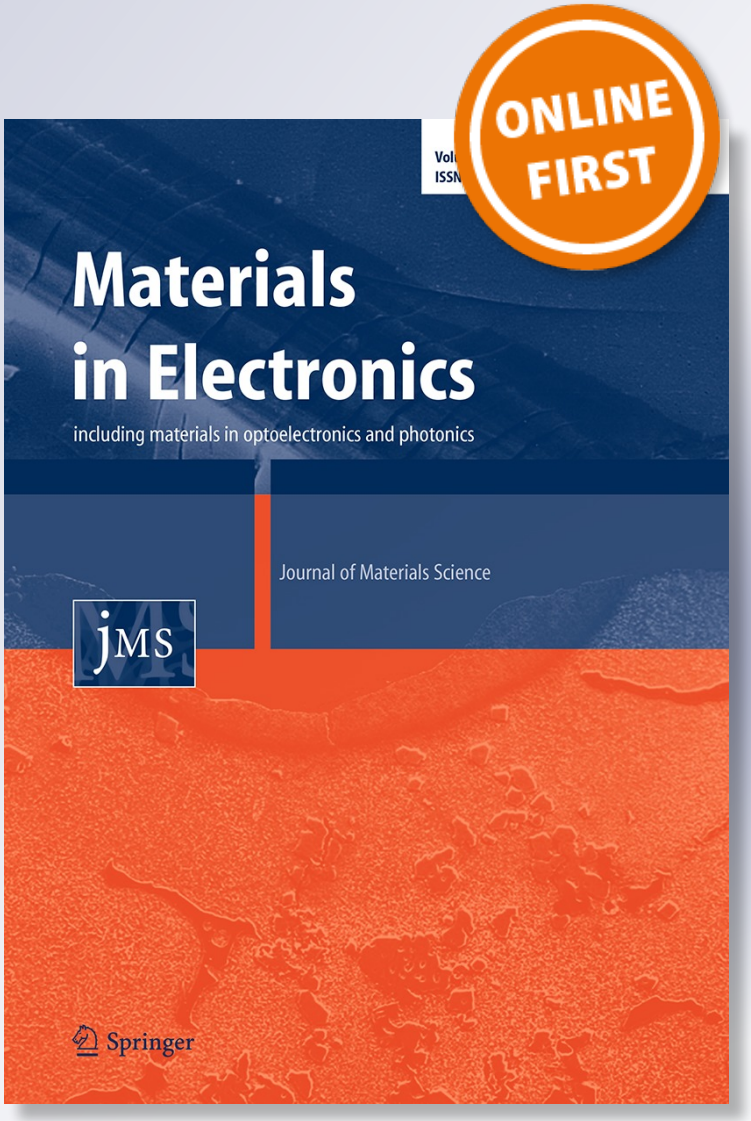

Springer

J Mater Sci: Mater Electron
DOI 10.1007/s10854-016-5316-5

The defect chemistry and dielectric properties of Sb_2O_3 doped non-stoichiometric barium strontium titanate ceramics

Chen Zhang[1] · Zhixin Ling[1] · Gang Jian[1]

Received: 10 May 2016 / Accepted: 4 July 2016

Abstract The microstructures and dielectric properties of Sb_2O_3 doped non-stoichiometric barium strontium titanate ceramics, prepared by solid state method, were investigated using XRD, SEM and LCR measure system. It is found that secondary phase and abnormal grain growth arise in the high Sb_2O_3 concentration doped non-stoichiometric barium strontium titanate ceramics. With the increase of Sb_2O_3 content, the relative dielectric constant at room temperature increases initially and then decreases while the dielectric loss at room temperature is determined by the concentration of oxygen vacancies $V_{\ddot{O}}$ and related defect complexes. The substitution preference of Sb^{3+} ion in non-stoichiometric barium strontium titanate ceramics changes according to the A-site ion/B-site ion mole ratio. The Curie temperature of $(Ba_{0.7}Sr_{0.3})Ti_{1.005}O_{3.01}$ and $(Ba_{0.7}Sr_{0.3})$-$Ti_{0.995}O_{2.99}$ ceramics increases and then decreases as the Sb_2O_3 content increases. The temperature stability of the relative dielectric constant for high concentration Sb_2O_3 doped non-stoichiometric barium strontium titanate ceramics deteriorates due to the weakened grain boundary buffering effect.

1 Introduction

Barium strontium titanate ($Ba_{1-x}Sr_xTiO_3$, BST) ferroelectric materials are well-known solid solutions which have shown great promise for applications as phase shifters, phased array antennas, resonators, capacitors, as well as gas sensors and thus intensively studied [1, 2]. High relative dielectric constant, low dielectric loss and good dielectric temperature stability are required for the "Y5V" or "X7R" capacitor applications. However, in the uniform BST ceramics there remains the conflict between the fine dielectric properties at room temperature and good dielectric temperature stability [3]. For solving this problem, the traditional doping method applied widely in electronic ceramics has been introduced into BST ceramics [4–6]. Due to the intermediate size and charge of trivalent ions compared to the Ba^{2+}, Sr^{2+} and Ti^{4+} ions, the aliovalent doping mechanism and substitution preference of trivalent ions in BST ceramics and in $BaTiO_3$ ceramics has been debated for many years [7]. In many cases, the doping mechanisms are not only dependent on the oxygen partial pressure (pO_2) and sintering temperature/time but also the overall A/B ratio [8]. And some influences of A/B ratio on the microstructures and dielectric properties in BST ceramics are gradually understood. Dong et al. [3] concluded that adding excessive TiO_2 could remarkably inhibit grain growth, suppress and broaden the Curie peaks in compositionally inhomogeneous BST ceramics. Syamaprasad et al. [9] found that excess Ba led to high unchanged dielectric constant with a slight decrease of tanδ in $Ba_{0.71}Sr_{0.29}TiO_3$ ceramics.

In our previous work, the dielectric properties of Sb_2O_3 doped stoichiometric BST ceramics such as $(Ba_{0.992-x}Sr_xY_{0.008})TiO_{3.004}$ ceramics(A/B ratio = 1) have been investigated [10, 11]. So in this article, we report a systematic study on the microstructure, defect behavior and dielectric properties of non-stoichiometric $(Ba_{0.7}Sr_{0.3})$-$Ti_{1.005}O_{3.01}$ ceramics (A/B ratio < 1) and $(Ba_{0.7}Sr_{0.3})$-$Ti_{0.995}O_{2.99}$ ceramics (A/B ratio > 1) still taking the trivalent Sb^{3+} ions as the dopant. The substitution

✉ Chen Zhang
czhang1981@hotmail.com

[1] Department of Materials Science and Engineering, Jiangsu University of Science and Technology, Zhenjiang 212003, China

Published online: 12 July 2016

preference of Sb^{3+} ion in perovskite lattice and the influence of Sb_2O_3 doping content on the temperature stability of the relative dielectric constant for non-stoichiometric barium strontium titanate ceramics are understood.

2 Experimental

The chemical compositions of the Sb_2O_3 doped non-stoichiometric barium strontium titanate specimens were given by the formula $(Ba_{0.7}Sr_{0.3})Ti_{1.005}O_{3.01}$ + x wt% Sb_2O_3 and $(Ba_{0.7}Sr_{0.3})Ti_{0.995}O_{2.99}$ + x wt% Sb_2O_3 (x = 0, 0.2, 0.4, 0.6, 0.8,1.0). High purity $BaCO_3$ (>99.0 %), $SrCO_3$ (>99.0 %) and TiO_2 (>98.0 %) powders used as starting raw materials were weighed according to the above formulas, ball-milled, dried and calcined at 1080 °C for 2 h. The calcined powders were mixed with Sb_2O_3 (>99.0 %), reground, dried and added with 5 wt% polyvinyl alcohol (PVA) as a binder for granulation. The mixture was sieved through 60-mesh screen and then pressed into pellets 10 mm in diameter and 2 mm in thickness under 250 Mpa. Sintering was conducted in air at 1320–1350 °C for 2 h. For dielectric measurement, both the flat surfaces of the specimens were coated with BQ-5311 silver paste after ultrasonic bath cleaning and then fired at 800 °C for 10 min.

The crystal structures of the specimens were confirmed by X-ray diffraction analysis (XRD, Rigaku D/max 2500v/pc) with Cu Kα radiation. The surface morphologies of the specimens were observed using the SEM (JSM-6480 ESEM). The capacitance quantity (C) and dissipation factor (D) were measured with LCR-8101G Automatic LCR Meter at 1 kHz.The relative dielectric constant (ε_r) and the loss tangent ($tan\delta$) were calculated as follows:

$$\varepsilon_r = \frac{14.4Ch}{\Phi^2} \quad (1)$$

$$\tan\delta = \frac{fD}{1000} \quad (2)$$

where h is the thickness (cm), Φ is the diameter of the electrode(cm) and f is the test frequency (Hz). An automatic measuring system consisting of Automatic LCR Meter and THP-F-100 temperature control unit was used to record the capacitance quantity (C) and dissipation factor (D) from −20 to 50 °C at 1 kHz for measuring the temperature dependence of dielectric parameters.

3 Results and discussion

The X-ray diffraction patterns of as sintered Sb_2O_3 doped $(Ba_{0.7}Sr_{0.3})Ti_{1.005}O_{3.01}$ bulk ceramics are shown in Fig. 1. As indicated in Fig. 1a, the undoped and 0.2 wt% Sb_2O_3 doped non-stoichiometric $(Ba_{0.7}Sr_{0.3})Ti_{1.005}O_{3.01}$ ceramics are single phase solid solutions with typical perovskite structure whose space group belong to Pm-3m(221). As the Sb_2O_3 doping content increases up to 0.4wt%, $(Ba_{0.7}Sr_{0.3})Ti_{1.005}O_{3.01}$ ceramics become multiphase compounds with monoclinic $Ba_2Ti_6O_{13}$ [space group C2/m(12)] as secondary phase. It demonstrates that in order to maintain the ABO_3 perovskite single phase structure the addition content of Sb_2O_3 in non-stoichiometric $(Ba_{0.7}Sr_{0.3})Ti_{1.005}O_{3.01}$ ceramics should be restricted to a much narrower range compared with that in stoichiometric $Ba_{0.672}Sr_{0.32}Y_{0.008}TiO_3$ ceramics [11]. The XRD profiles focusing on the (111) diffraction peaks are presented in Fig. 1b. With the increase of Sb_2O_3 content, a slight shift of diffraction peaks for the primary perovskite phase to higher two-theta values is observed, which indicates that the unit cell volumes of perovskite phase decrease as the Sb_2O_3 addition content increases. Similar phenomenon has been previously reported in Ca substituted BST ceramics [12] and in our previous work for (La, Sb)-doped $(Ba_{0.74}Sr_{0.26})TiO_3$

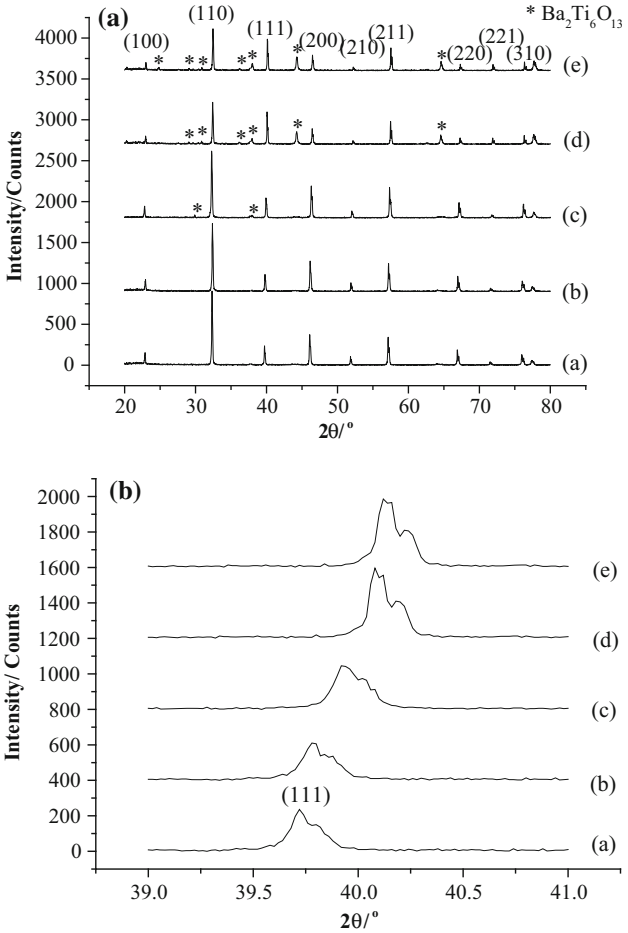

Fig. 1 XRD patterns for Sb_2O_3 doped $(Ba_{0.7}Sr_{0.3})Ti_{1.005}O_{3.01}$ ceramics: **a** 0 wt% Sb_2O_3; **b** 0.2 wt% Sb_2O_3; **c** 0.4 wt% Sb_2O_3; **d** 0.6 wt% Sb_2O_3; **e** 0.8 wt% Sb_2O_3

ceramics [13]. The ionic radii of Ba^{2+}, Sr^{2+} in 12 coordination and Ti^{4+} in 6 coordination are 0.161 nm, 0.144 nm and 0.061 nm, respectively. The radius of Sb^{3+} ion in 6 coordination (0.076 nm) is bigger than that of Ti^{4+} ion but smaller than that of host A-site ions. The above shrinkage of unit cell suggests that the Sb^{3+} ions enter into the A-sites of perovskite lattice rather than B-sites in $(Ba_{0.7}Sr_{0.3})Ti_{1.005}O_{3.01}$ ceramics.

Figure 2 shows the surface morphologies of Sb_2O_3 doped $(Ba_{0.7}Sr_{0.3})Ti_{1.005}O_{3.01}$ ceramics. It appears that the $(Ba_{0.7}Sr_{0.3})Ti_{1.005}O_{3.01}$ samples without the Sb_2O_3 dopant or with low Sb_2O_3 concentration exhibit dense microstructures and fine grain size distribution. However, the abnormal grain growth and the cylindrical grains which indicate the precipitation of secondary phase exist in the 0.8 wt% Sb_2O_3 doped $(Ba_{0.7}Sr_{0.3})Ti_{1.005}O_{3.01}$ ceramics.

Figure 3 shows the relative dielectric constant and dielectric loss of $(Ba_{0.7}Sr_{0.3})Ti_{1.005}O_{3.01}$ ceramics as a function of Sb_2O_3 content at room temperature. It is obvious that all the non-stoichiometric $(Ba_{0.7}Sr_{0.3})Ti_{1.005}O_{3.01}$ ceramics possess high relative dielectric constant (more than 2200) and low dielectric loss (less than 0.008) at room temperature. With the increase of Sb_2O_3 content, the relative dielectric constant increases initially and then decreases. The maximum of relative dielectric constant at room temperature can be found in 0.8 wt% Sb_2O_3 doped $(Ba_{0.7}Sr_{0.3})Ti_{1.005}O_{3.01}$ ceramics. The dielectric loss of $(Ba_{0.7}Sr_{0.3})Ti_{1.005}O_{3.01}$ ceramics increases with the increasing Sb_2O_3 content.

Temperature dependence of the relative dielectric constant for Sb_2O_3 doped $(Ba_{0.7}Sr_{0.3})Ti_{1.005}O_{3.01}$ ceramics is shown in Fig. 4. The relative dielectric constant first increases, achieves a maximum (ε_{rmax}) and then decreases with increasing temperature. The temperature corresponding to the relative dielectric constant maximum is taken as the Curie temperature. It is obvious that the Curie temperature shifts to higher value and then decreases with increasing Sb_2O_3 doping concentration. As indicated in Fig. 4, the Curie temperature for 0.4 wt% Sb_2O_3 doped $(Ba_{0.7}Sr_{0.3})Ti_{1.005}O_{3.01}$ ceramics is −6 °C. The Curie temperature for 0.8 wt% Sb_2O_3 doped $(Ba_{0.7}Sr_{0.3})Ti_{1.005}O_{3.01}$ ceramics is −1 °C while that for 1.0 wt% Sb_2O_3 doped $(Ba_{0.7}Sr_{0.3})Ti_{1.005}O_{3.01}$ ceramics is −7 °C. Furthermore, ε_{rmax} is also enhanced and then restrained with the increase of Sb_2O_3 content. The above two phenomena are mainly attributed to the variation in perovskite lattice

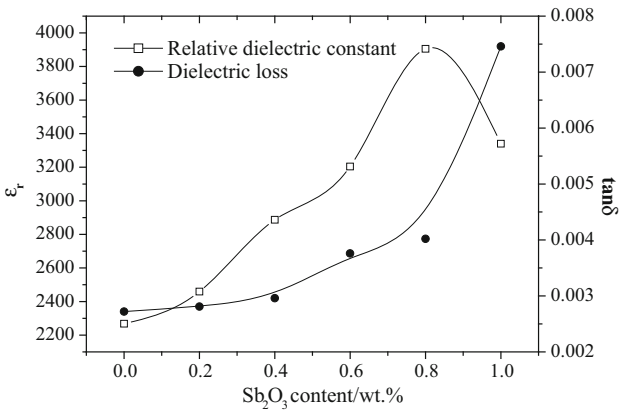

Fig. 3 Relative dielectric constant and dielectric loss of $(Ba_{0.7}Sr_{0.3})Ti_{1.005}O_{3.01}$ ceramics as a function of Sb_2O_3 content at 1 kHz

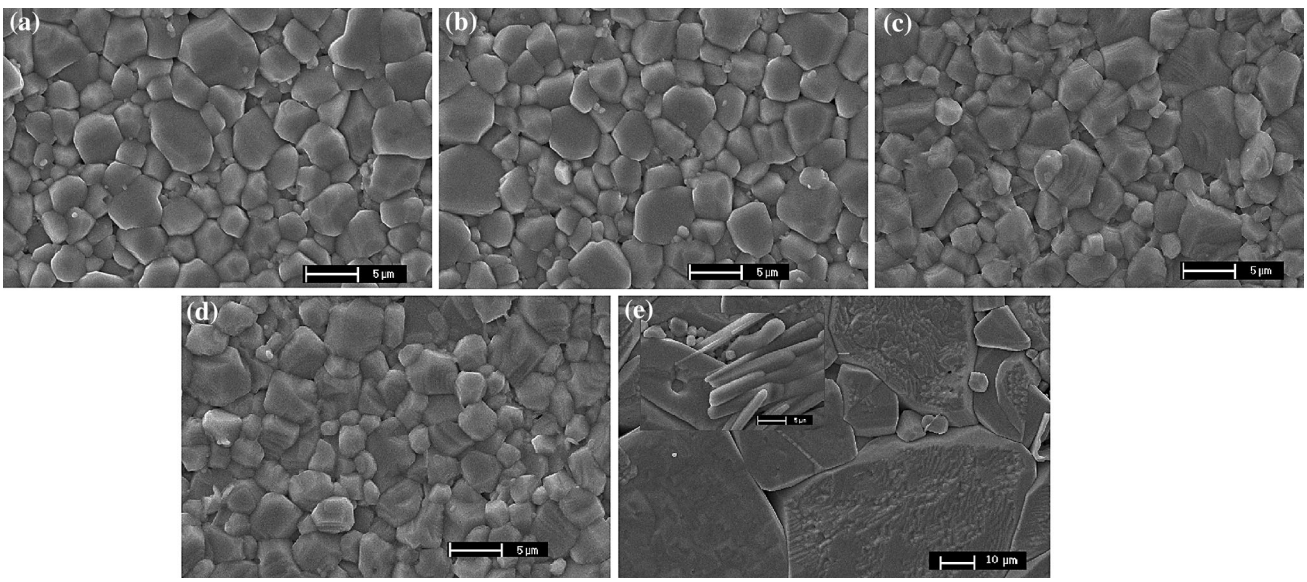

Fig. 2 SEM micrographs of Sb_2O_3 doped $(Ba_{0.7}Sr_{0.3})Ti_{1.005}O_{3.01}$ ceramics: **a** $Sb_2O_3 = 0$ wt%; **b** $Sb_2O_3 = 0.2$ wt%; **c** $Sb_2O_3 = 0.4$ wt%; **d** $Sb_2O_3 = 0.6$ wt%; **e** $Sb_2O_3 = 0.8$ wt%

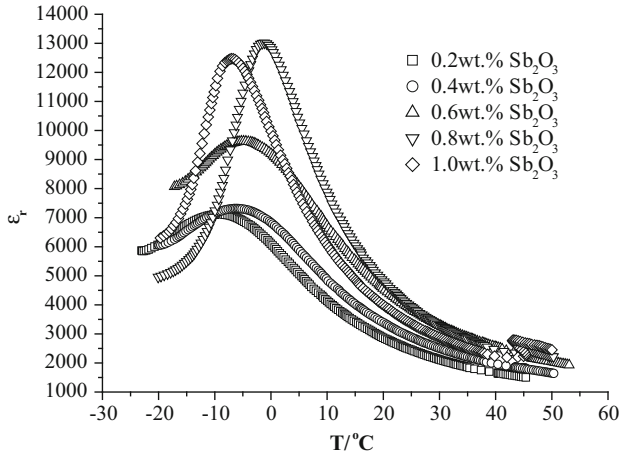

Fig. 4 Temperature dependence of relative dielectric constant for Sb_2O_3 doped $(Ba_{0.7}Sr_{0.3})Ti_{1.005}O_{3.01}$ ceramics

structure caused by the occupation of Sb^{3+} ions in A-sites. In non-stoichiometric $(Ba_{0.7}Sr_{0.3})Ti_{1.005}O_{3.01}$ ceramics (A/B ratio < 1), there is severe lattice deformation due to the appearance of A-site vacancies V_A'' and oxygen vacancies $V_O^{\cdot\cdot}$ which is revealed by the following point defect reaction equation:

$$(Ba_{0.7}Sr_{0.3})Ti_{1.005}O_{3.01} \rightarrow 0.7Ba_{Ba} + 0.3Sr_{Sr} + 1.005Ti_{Ti} + 3.01O_O + 0.005V_A'' + 0.005V_O^{\cdot\cdot} \quad (3)$$

After doping Sb_2O_3 in the $(Ba_{0.7}Sr_{0.3})Ti_{1.005}O_{3.01}$ ceramics, Sb^{3+} ions gradually enter the A-sites in perovskite lattice and correspondingly fill up the A-site vacancies V_A'' initially, which weakens the existing lattice deformation and leads to a longer distance between the central ion and its nearest neighbors of the oxygen octahedron. Therefore, the movement of the central ion is relatively less confined, which enhances the spontaneous polarization of the perovskite grain lattice. It is exactly the increased spontaneous polarization that takes responsibility of the increasing Curie temperature and ε_{rmax}. As the Sb_2O_3concentration continues to increase, A-site ions in the perovskite lattice start to be partially substituted by smaller Sb^{3+} ions, consequently causing even worse lattice deformation and a shorter distance between the central ion and its nearest neighbours of the octahedron. Apparently, the decrease of Curie temperature and ε_{rmax} in high Sb_2O_3 content doped $(Ba_{0.7}Sr_{0.3})Ti_{1.005}O_{3.01}$ ceramics is attributed to the weakening of spontaneous polarization of the grain lattice induced by the substitution for host ion with any of the Sb^{3+} ions. The variation of the intensity of spontaneous polarization also provides an explanation for the changing of relative dielectric constant at room temperature shown in Fig. 3. Since the previously mentioned shrinkage of the unit cell implies the substitution of Sb^{3+} ions for the A-site ions in $(Ba_{0.7}Sr_{0.3})Ti_{1.005}O_{3.01}$ samples with high Sb_2O_3 concentration, the following defect reaction takes place:

$$Sb_2O_3 \rightarrow 2Sb_A^{\cdot} + V_A'' + 3O_O \quad (4)$$

Oxygen vacancies $V_O^{\cdot\cdot}$ residing at the corners of the octahedra in non-stoichiometric $(Ba_{0.7}Sr_{0.3})Ti_{1.005}O_{3.01}$ ceramics are well interconnected and therefore can be regarded as relatively "mobile" defects. The mobile defects migrate to domain boundaries. Orientation of the elastic dipoles caused by $V_O^{\cdot\cdot}$ and the electric dipoles formed from $V_A'' - V_O^{\cdot\cdot}$ complexes shown in Eq. (3) results in the domain-wall pinning and thus the un-doped $(Ba_{0.7}Sr_{0.3})Ti_{1.005}O_{3.01}$ ceramics possess a low dielectric loss at room temperature. As the Sb_2O_3 addition content increases, A-site vacancies V_A'' and oxygen vacancies $V_O^{\cdot\cdot}$ are occupied by Sb^{3+} ions and O^{2-} ions respectively as mentioned earlier, which makes the concentration of V_A'' and $V_O^{\cdot\cdot}$ decrease and then the domain-wall pinning destroyed. Therefore, the dielectric loss of $(Ba_{0.7}Sr_{0.3})Ti_{1.005}O_{3.01}$ ceramics increases with the increasing Sb_2O_3 content.

The X-ray diffraction patterns of as sintered Sb_2O_3 doped $(Ba_{0.7}Sr_{0.3})Ti_{0.995}O_{2.99}$ bulk ceramics are shown in Fig. 5. When the Sb_2O_3 doping concentration is less than 0.8 wt%, $(Ba_{0.7}Sr_{0.3})Ti_{0.995}O_{2.99}$ ceramics are single phase solid solutions with typical perovskite structure while the centrosymmetric compound $Ti_{10}O_{19}$ is formed as a secondary phase in the 1.0 wt% Sb_2O_3 doped $(Ba_{0.7}Sr_{0.3})Ti_{0.995}O_{2.99}$ ceramics. No secondary phase containing Sb was found in present samples, implying that the Sb^{3+} dopant ions entered the perovskite structure rather than contributed to the formation of secondary phases. It is notable that the solid solubility of Sb_2O_3 in single phase non-stoichiometric $(Ba_{0.7}Sr_{0.3})Ti_{0.995}O_{2.99}$ ceramics is higher than that in single phase $(Ba_{0.7}Sr_{0.3})Ti_{1.005}O_{3.01}$ ceramics. With the increase of Sb_2O_3 content, a slight shift of diffraction peaks for the primary perovskite phase to lower values is observed in Fig. 5b, which indicates that the unit cell volumes of $(Ba_{0.7}Sr_{0.3})Ti_{0.995}O_{2.99}$ ceramics increase as the Sb_2O_3 addition content increases. In terms of the radii of the host ions and Sb^{3+} ions, the expanded unit cell implies that Sb^{3+} ions prefer to occupy the B-sites rather than A-sites in $(Ba_{0.7}Sr_{0.3})Ti_{0.995}O_{2.99}$ ceramics.

Figure 6 shows the surface morphologies of Sb_2O_3 doped $(Ba_{0.7}Sr_{0.3})Ti_{0.995}O_{2.99}$ ceramics. With the increase of Sb_2O_3 concentration, the average grain size of $(Ba_{0.7}Sr_{0.3})Ti_{0.995}O_{2.99}$ samples increases and the dense microstructures as well as fine grain size distribution are obtained even in 0.8 wt% Sb_2O_3 doped $(Ba_{0.7}Sr_{0.3})Ti_{0.995}O_{2.99}$ ceramics. However, the abnormal grain growth and the cylindrical grains which indicate the appearance of secondary phase exist in the 1.0 wt% Sb_2O_3 doped $(Ba_{0.7}Sr_{0.3})Ti_{0.995}O_{2.99}$ ceramics.

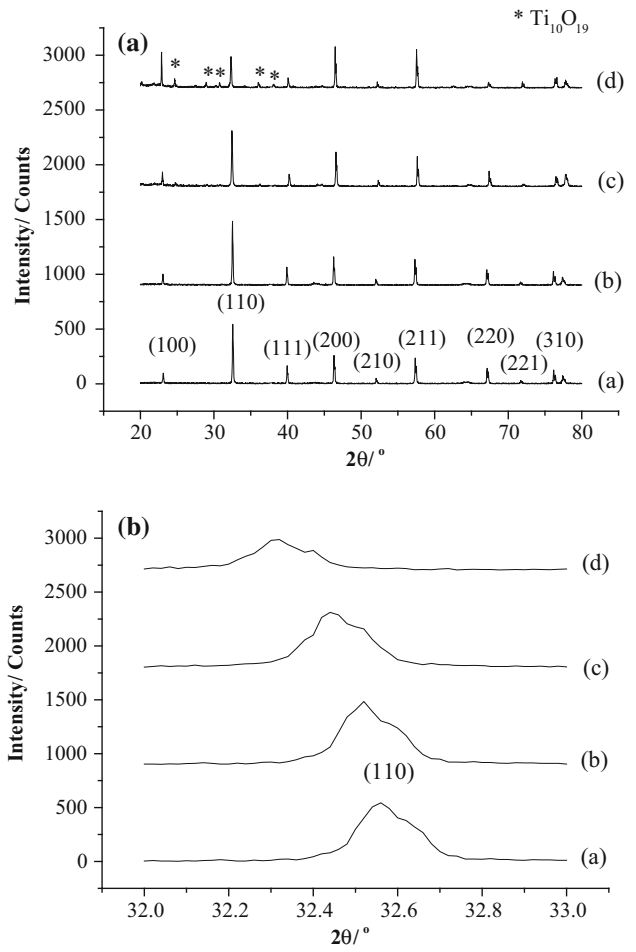

Fig. 5 XRD patterns for Sb_2O_3 doped $(Ba_{0.7}Sr_{0.3})Ti_{0.995}O_{2.99}$ ceramics: **a** 0 wt% Sb_2O_3; **b** 0.4 wt% Sb_2O_3; **c** 0.8 wt% Sb_2O_3; **d** 1.0 wt% Sb_2O_3

Figure 7 shows the relative dielectric constant and dielectric loss of $(Ba_{0.7}Sr_{0.3})Ti_{0.995}O_{2.99}$ ceramics as a function of Sb_2O_3 content at room temperature. With the increase of Sb_2O_3 content, the relative dielectric constant increases initially and then decreases. The maximum of the relative dielectric constant at room temperature can be found in 0.6 wt% Sb_2O_3 doped $(Ba_{0.7}Sr_{0.3})Ti_{0.995}O_{2.99}$ ceramics. The dielectric loss of $(Ba_{0.7}Sr_{0.3})Ti_{0.995}O_{2.99}$ ceramics increases and then diminishes with the increasing Sb_2O_3 content.

Temperature dependence of relative dielectric constant for Sb_2O_3 doped $(Ba_{0.7}Sr_{0.3})Ti_{0.995}O_{2.99}$ ceramics is shown in Fig. 8. It is found that the Curie temperature of $(Ba_{0.7}Sr_{0.3})Ti_{0.995}O_{2.99}$ ceramics increases and then decreases with the increasing Sb_2O_3 content. In non-stoichiometric $(Ba_{0.7}Sr_{0.3})Ti_{0.995}O_{2.99}$ ceramics (A/B ratio > 1), the severe lattice deformation also shows up due to the existing of B-site vacancies V_{Ti}'''' and oxygen vacancies $V_O^{\cdot\cdot}$ which is revealed by the following point defect reaction equation:

$$(Ba_{0.7}Sr_{0.3})Ti_{0.995}O_{2.99} \rightarrow 0.7Ba_{Ba} + 0.3Sr_{Sr} + 0.995Ti_{Ti} + 2.99O_O + 0.005V_{Ti}'''' + 0.01V_O^{\cdot\cdot} \quad (5)$$

After incorporating Sb_2O_3 in the $(Ba_{0.7}Sr_{0.3})Ti_{0.995}O_{2.99}$ ceramics, Sb^{3+} ions occupy the B-site vacancies V_{Ti}'''' at first, which weakens the lattice deformation and increases the spontaneous polarization. Obviously, this is in accord with the variation of spontaneous polarization in $(Ba_{0.7}Sr_{0.3})Ti_{1.005}O_{3.01}$ ceramics when Sb^{3+} ions fill up the A-site vacancies V_A''. The enhanced spontaneous polarization

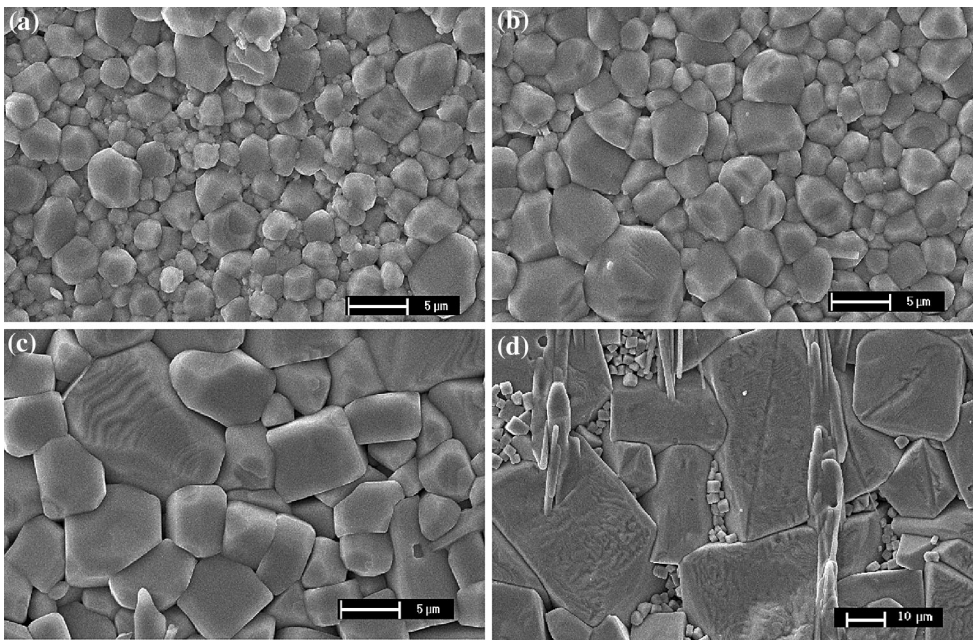

Fig. 6 SEM micrographs of Sb_2O_3 doped $(Ba_{0.7}Sr_{0.3})Ti_{0.995}O_{2.99}$ ceramics: **a** $Sb_2O_3 = 0$ wt%; **b** $Sb_2O_3 = 0.4$ wt%; **c** $Sb_2O_3 = 0.8$ wt%; **d** $Sb_2O_3 = 1.0$ wt%

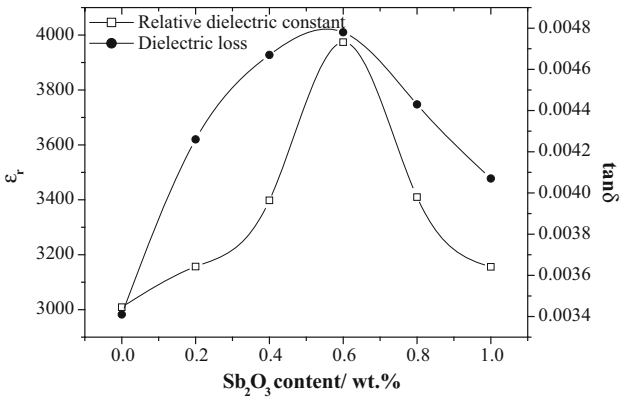

Fig. 7 Relative dielectric constant and dielectric loss of $(Ba_{0.7}Sr_{0.3})Ti_{0.995}O_{2.99}$ ceramics as a function of Sb_2O_3 content at 1 kHz

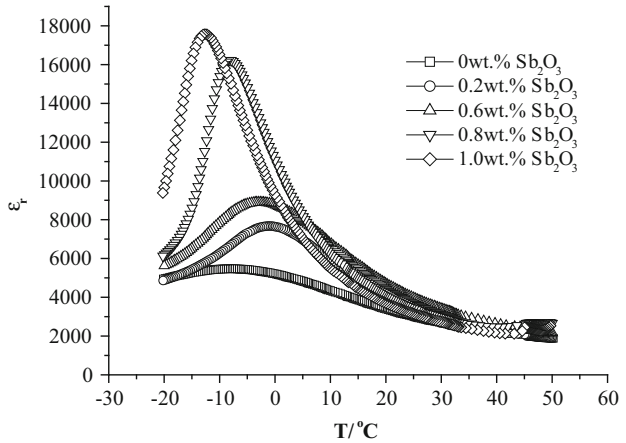

Fig. 8 Temperature dependence of relative dielectric constant for Sb_2O_3 doped $(Ba_{0.7}Sr_{0.3})Ti_{0.995}O_{2.99}$ ceramics

finally leads to the increasing Curie temperature. As the Sb_2O_3 content increases, Sb^{3+} ions turn to substitute the B-site ions in $(Ba_{0.7}Sr_{0.3})Ti_{0.995}O_{2.99}$ samples, which can be inferred from the increase in the unit cell volume. Correspondingly, the following defect reaction takes place:

$$Sb_2O_3 \rightarrow 2Sb'_{Ti} + V_O^{\cdot\cdot} + 3O_O \quad (6)$$

The substitution for B-site host ions with any of the Sb^{3+} ions contributes to the lattice deformation and shorter distance between the central ion and its nearest neighbors of the octahedron. The weakened spontaneous polarization arising from the substitution for host ions correspondingly decreases the Curie temperature of present $(Ba_{0.7}Sr_{0.3})Ti_{0.995}O_{2.99}$ ceramics.

As the Sb_2O_3 addition content increases, B-site vacancies V_{Ti}'''' and oxygen vacancies $V_O^{\cdot\cdot}$ shown in Eq. (5) are filled by Sb^{3+} ions and O^{2-} ions respectively, which gives rise to the decrease of V_{Ti}'''' and $V_O^{\cdot\cdot}$ concentration. When the substitution of Sb^{3+} ions for B-site ions shown in Eq. (6) takes place, the additional oxygen vacancies $V_O^{\cdot\cdot}$ are brought about, making the concentration of $V_O^{\cdot\cdot}$ bounce back. Correspondingly, the domain-wall pinning effect caused by the orientation of the elastic dipoles and the electric dipoles formed from $V_{Ti}'''' - V_O^{\cdot\cdot}$ complexes is weakened and then enhanced with the increasing Sb_2O_3 content. Therefore, the dielectric loss of $(Ba_{0.7}Sr_{0.3})$-$Ti_{0.995}O_{2.99}$ ceramics increases and then decreases with the increase of Sb_2O_3 content.

Based on the above, it is presented that the substitution preference of Sb^{3+} ions in $(Ba_{0.7}Sr_{0.3})Ti_{1.005}O_{3.01}$ (A/B ratio < 1) and $(Ba_{0.7}Sr_{0.3})Ti_{0.995}O_{2.99}$ (A/B ratio > 1) perovskite structure is different from each other. It is clear that in non-stoichiometric barium strontium titanate ceramics with B-site vacancies V_{Ti}'''', Sb^{3+} ions tend to enter the B-sites while in those with A-site vacancies V_A'', Sb^{3+} ions prefer to occupy the A-sites of perovskite lattice.

As shown in Fig. 8, the temperature stability of relative dielectric constant for high concentration Sb_2O_3 doped $(Ba_{0.7}Sr_{0.3})Ti_{0.995}O_{2.99}$ ceramics is worse than that for low concentration doped ones. It can be explained using the so called grain boundary buffering theory. The diffusion of non-ferroelectric grain boundaries among the barium strontium titanate ferroelectric grains helps the orientation of ferroelectric domain below the Curie temperature which makes the ferroelectric-paraelectric phase transition taking place in a relative broad temperature range. The average grain size of $(Ba_{0.7}Sr_{0.3})Ti_{0.995}O_{2.99}$ samples increases with the increasing Sb_2O_3 concentration as mentioned previously. This means that the portion of grain boundary decrease with the increasing Sb_2O_3 concentration and consequently the grain boundary buffering effect becomes insignificant. Macroscopically, the Curie peak for high Sb_2O_3 concentration samples is sharper than that for low Sb_2O_3 concentration ones.

4 Conclusions

The microstructures and dielectric properties, especially the relationships between the point defect and dielectric properties, were investigated by XRD, SEM and LCR measure system for Sb_2O_3 doped non-stoichiometric $(Ba_{0.7}Sr_{0.3})Ti_{1.005}O_{3.01}$ (A/B ratio < 1) and $(Ba_{0.7}Sr_{0.3})Ti_{0.995}O_{2.99}$ (A/B ratio > 1) ceramics prepared by conventional solid state method for low frequency capacitor applications. It is found that secondary phase and abnormal grain growth show up in the high Sb_2O_3 concentration doped non-stoichiometric barium strontium titanate ceramics. The relative dielectric constant at room temperature increases initially and then decreases with the increase of Sb_2O_3 content. The dielectric loss at room

temperature is determined by the concentration of oxygen vacancies $V_O^{\cdot\cdot}$ and related defect complexes. The A/B ratio and thus the existing defect in perovskite structure become the controlling factor for substitution preference of Sb^{3+} ion in non-stoichiometric barium strontium titanate ceramics. It is revealed that the Curie temperature of $(Ba_{0.7}Sr_{0.3})Ti_{1.005}O_{3.01}$ and $(Ba_{0.7}Sr_{0.3})Ti_{0.995}O_{2.99}$ ceramics increases and then decreases as the Sb_2O_3 content increases. The weakened grain boundary buffering effect takes responsibility for the poor temperature stability of the relative dielectric constant for high concentration Sb_2O_3 doped non-stoichiometric barium strontium titanate ceramics.

Acknowledgments This work is supported by the Project Funded by the Priority Academic Program Development of Jiangsu Higher Education Institutions and sponsored by Suzhou Pante Electric Ceramics Tech. Co. Ltd. This work is also supported by Natural Science Foundation of Jiangsu Province in China (BK20140517) and University Natural Science Project of Jiangsu Province in China (14KJB430011).

References

1. S. Dupuis, S. Sulekar, J.H. Kim, H. Han, P. Dufour, C. Tenailleau, J.C. Nino, S. Guillemet-Fritsch, J. Eur. Ceram. Soc. **36**, 567 (2016)
2. A.K. Tagantsev, V.O. Sherman, K.F. Astafiev, J. Venkatesh, N. Setter, J. Electroceram. **11**, 5 (2003)
3. H. Dong, D. Jin, C. Xie, J. Cheng, L. Zhou, J. Chen, Mater. Lett. **135**, 83 (2014)
4. B. Su, T.W. Button, J. Appl. Phys. **95**, 1382 (2004)
5. Y. Li, Y. Qu, Mater. Res. Bull. **44**, 82 (2009)
6. S. Liu, V.Y. Zenou, I. Sus, T. Kotani, M. Schilfgaarde, N. Newman, Acta Mater. **55**, 2647 (2007)
7. C.L. Freeman, J.A. Dawson, H.R. Chen, L. Ben, J.H. Harding, F.D. Morrison, D.C. Sinclair, A.R. West, Adv. Funct. Mater. **23**, 3925 (2013)
8. H. Kishi, Y. Mizuno, H. Chazono, J. Appl. Phys. **42**, 1 (2003)
9. U. Syamaprasad, R.K. Galgali, B.C. Mohanty, Mater. Lett. **8**, 36 (1989)
10. C. Zhang, Y. Qu, S. Ma, Mater. Sci. Eng. B **136**, 118 (2007)
11. C. Zhang, Y. Qu, S. Ma, Mater. Lett. **61**, 1007 (2007)
12. S. Yun, X. Wang, B. Li, D. Xu, Solid State Commun. **143**, 461 (2007)
13. C. Zhang, Y. Qu, Trans. Nonferr. Met. Soc. China **22**, 2742 (2012)